Supporting Information

Oriented Synthesis of Pyridinic-N Dopant within the Highly Efficient Multifunction Carbon-Based Materials for Oxygen Transformation and Energy Storage

Fantao Kong†, Yu Qiao†, Chaoqi Zhang†, Xiaohong Fan†, Qingbiao Zhao‡*, Aiguo Kong†* and Yongkui Shan†*

†School of Chemistry and Molecular Engineering, East China Normal University, Dongchuan Road No. 500, Minhang District, Shanghai 200241, P. R. China
‡Key Laboratory of Materials and Devices, Department of Electronic Science, East China Normal University, Dongchuan Road No. 500, Minhang District, Shanghai 200241, P. R. China

*Corresponding author.
E-mail address:
agkong@chem.ecnu.edu.cn,ykshan@chem.ecnu.edu.cn,qbzhao@ee.ecnu.edu.cn

Number of pages: 12

Number of figures: 7

Number of tables: 5

CONTENTS

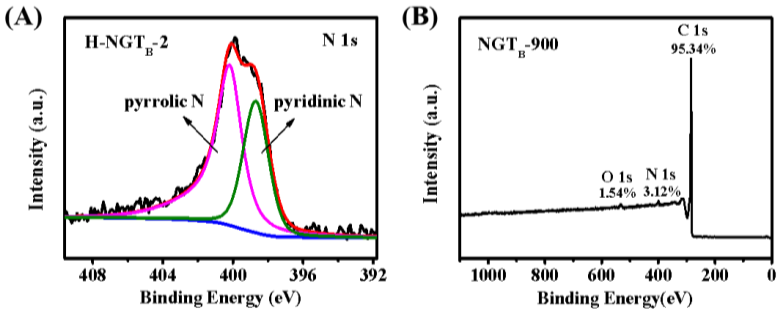

Figure S1. (A) N1s high-resolution XPS spectrum of the H-NCT$_B$-2 along with the corresponding fitting curves; (B) The survey XPS spectrum of the NGT$_B$-900.

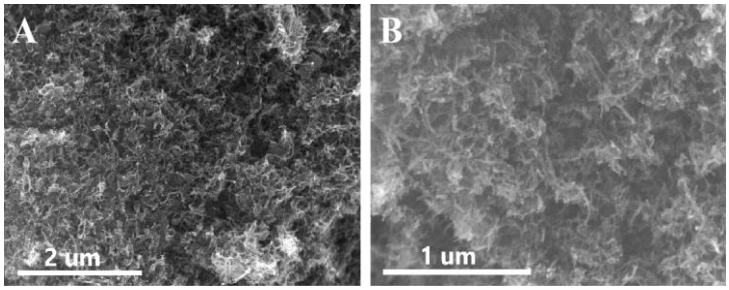

Figure S2. (A, B) SEM images of the freeze-dried H-NGT$_B$ samples.

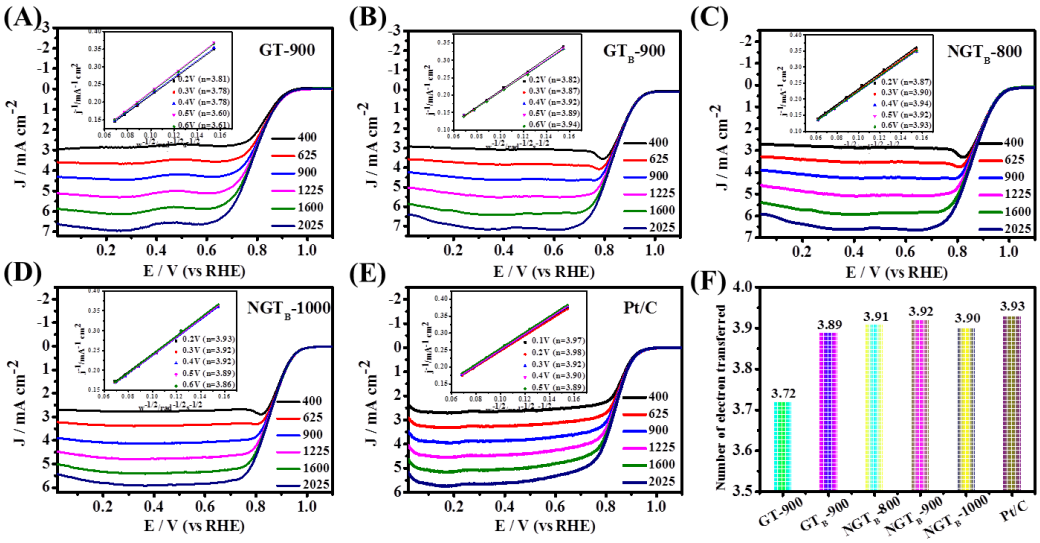

Figure S3. (A-E) LSV curves and electron transfer numbers (n) for the prepared GT-900, GT$_B$-900, NGT$_B$-800, -1000 samples and Pt/C with different rotating rate in O_2-saturated 0.1 M KOH solution; (F) Comparison between numbers of electron transferred per O_2 in ORR on different samples.

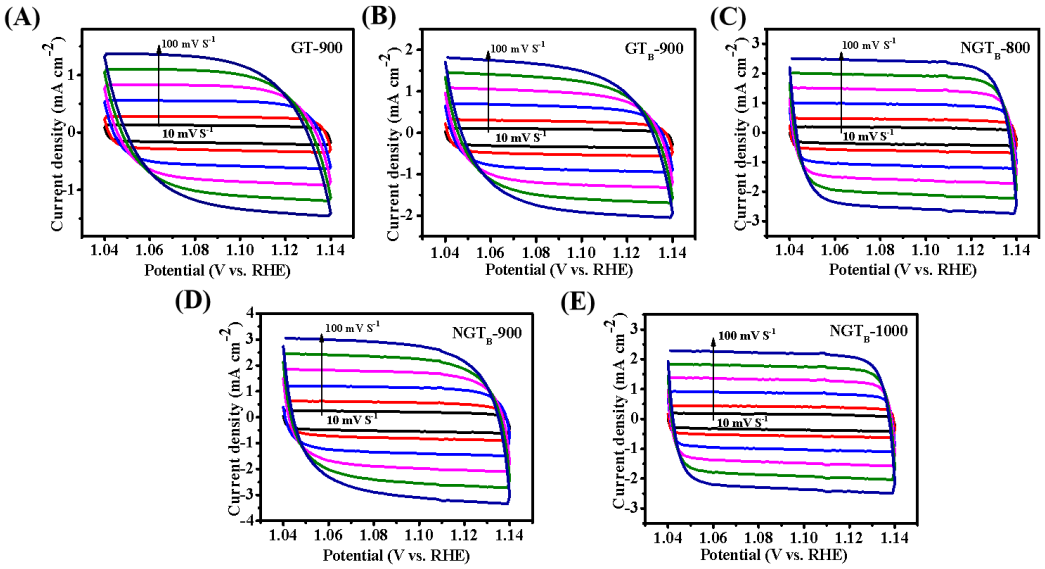

Figure S4. Cyclic voltammetry (CV) of GT-900 (A), GT_B-900 (B), NGT_B-800 (C), NGT_B-900 (D), and NGT_B-1000 (E) with different scan rates from 10 to 100 $mV \cdot s^{-1}$ in a non-faradic potential range of 1.04~1.14 V *vs.* RHE in 0. 1 M KOH solution.

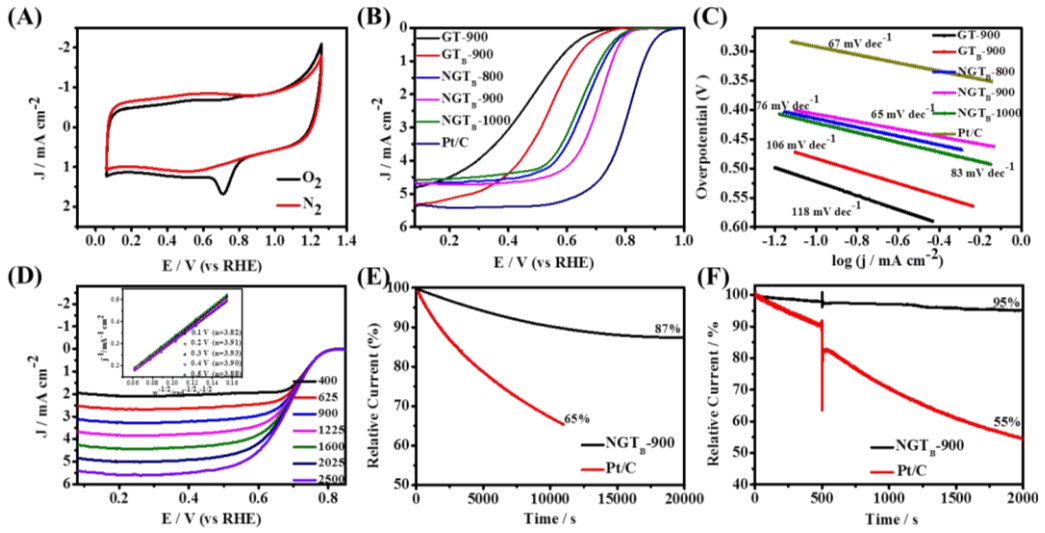

Figure S5. (A) CV curves of NGT_B-900 and Pt/C in O_2- or N_2-saturated 0.1 M $HClO_4$ solution; (B) LSV polarization curves and (C) the corresponding Tafel slope curves of ORR on different samples in O_2-saturated 0.1 M $HClO_4$ solution; (D) LSV curves and electron transfer number (n) of the prepared NGT_B-900 with different rotating rate in O_2-saturated 0.1 M $HClO_4$ solution; (E) Current-time (i-t) chronoamperometric response of NGT_B-900 and Pt/C-JM

in O_2-saturated 0.1 M $HClO_4$ at a rotation rate of 1600 rpm on the RDE electrode; (F) Current-time (i-t) chronoamperometric response of NGT_B-900 and Pt/C-JM with the addition of methanol (3 wt %) in O_2-saturated 0.1 M $HClO_4$ sulution at a rotation rate of 1600 rpm on the RDE electrode.

The electrocatalytic performance of the prepared catalysts for ORR was also evaluated in 0.1 M $HClO_4$ electrolyte. As shown in Figure 6A, a well-defined cathodic redox peak can be observed at 0.71 V (vs. RHE) on the NGT_B-900 in O_2-saturated 0.1 M $HClO_4$ solution, but no evident peak is recorded in N_2-saturated solution, which exhibits the effective ORR activity of NGT_B-900 in acidic condition. LSV curves in Figure 6B show that NGT_B-900 possesses superior ORR activity with a half-wave potential of 0.70 V, which is more positive than those on GT-900 (0.46 V), GT_B-900 (0.53 V), NGT_B-800 (0.66 V), NGT_B-1000 (0.64 V) and close to that on the commercial Pt/C (0.80 V). Actually, the electrocatalytic activity of NGT_B-900 toward ORR in acidic solution also shows advantages over the most of N-doped carbon materials reported in literature.[1-4] In the corresponding Tafel curves (Figure. 6C), Tafel slope (65 mV dec^{-1}) of ORR on NGT_B-900 is smaller than those on GT-900 (118 mV dec^{-1}), GT_B-900 (106 mV dec^{-1}), NGT_B-800 (76 mV dec^{-1}), NGT_B-1000 (83 mV dec^{-1}) and Pt/C (67 mV dec^{-1}), indicating a quicker reaction rate on the NGT_B-900. The limit current density of ORR on NGT_B-900 increases with the rate of rotation (Figure 6D). The linearly fitted K-L plots were obtained based on the K-L equation (inset of Figure 6D), illustrating similar electron transfer mechanism for ORR at the various potentials and a first-order reaction kinetic relative to the concentration of dissolved O_2. In the potential range of 0.1-0.5 V, the average numbers (n) of electron transferred is ~3.90, implying that NGT_B-900 undergoes a nearly $4e^-$ oxygen reduction reaction pathway. As demonstrated in Figure 6E, NGT_B-900 shows a long-term durability with 87% retention of initial current density after 20,000 s, which is superior to that on Pt/C (65% retention of initial current density after 10,000 s).

The NGT_B-900 also shows a good methanol tolerance in acidic solution (Figure 6F), as evidenced by almost no change in the current density after injection of 3% methanol at the time node of 500s, while a remarkable decline (~45%) can be observed in the current density of ORR on Pt/C electrode, which is resulted from the toxic effect of methanol.

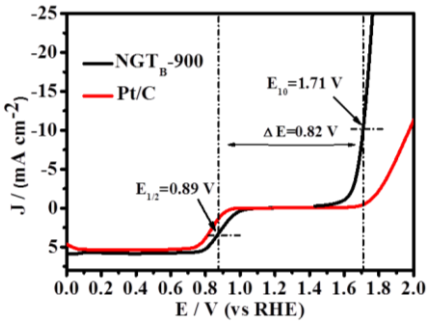

Figure S6. The overall polarization curves of NGT_B-900 and commercial Pt/C catalysts in O_2-saturated 0.1 M KOH solution for ORR/OER.

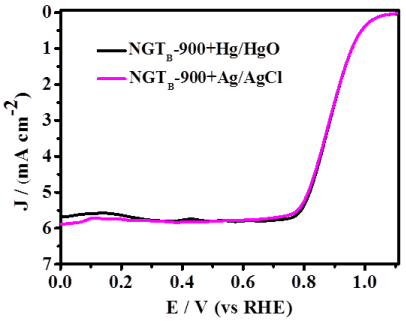

Figure S7. The LSV curves of NGT_B-900 for ORR using Hg/HgO or Ag/AgCl as reference electrode.

The contrast experiments were carried out to investigate the electrocatalytic activity of NGT_B-900 catalyst for ORR using a Hg/HgO as a reference electrode. As can be seen from Figure S7, the difference of ORR activity on NGT_B-900 catalyst using Hg/HgO as reference electrode from that using Ag/AgCl as reference electrode is negligible in 0.1 M KOH solution. This result confirms that Ag/AgCl electrode is stable and suitable in alkaline medium.

Table S1. Analysis of the nitrogen species in N-doped carbon-based metal-free catalysts reported in the literature.

Methods	N functional groups (%)				Refs.
	N1	N2	N3	N4	
CVD (3.1 at.%)	62.0%	38.0%	—	—	J. Catal. 311 (2014) 80-87
ball milling (3.15 at.%)	21.3%	73.1%	5.6%	—	J. Power Sources 342 (2017) 157-164.
plasma discharge (4.1 at.%)	10.0%	—	73.2%	16.8%	Carbon 100 (2016) 337-344
arc-discharge (6.5 at.%)	40.0%	46.2%	—	13.8%	Appl. Surf. Sci. 277 (2013) 88-93
solvothermal (6.34 at.%)	32.8%	41.9%	25.3%	—	Int. J. Hydrogen Energy 39 (2014) 6845-6852
wet chemical method (7.65 at.%)	35.4%	39.6%	17.6%	7.4%	J. Power Sources 227 (2013) 185-190
thermal annealing (2.9 at.%)	44.8%	13.8%	20.7%	20.7%	Sci. Adv. 1 (2015) e1400129
ion sputtering (0.7 at.%)	95.0%	—	5.0%	—	Science 351 (2016) 361-365
this method (3.12 at.%)	84.3%	—	15.7%	—	This work

Notes：N1, Pyridinic-N; N2, Pyrrolic-N; N3, Graphitic-N; N4, Oxidized nitrogen. Figures in parenthesis refer to the total nitrogen content.

Table S2. The surface element composition of NGT_B-n from the XPS analysis.

Samples	Element composition (at. %)		
	C	O	N
NGT_B-800	93.76	1.78	4.46
NGT_B-900	95.34	1.54	3.12
NGT_B-950	97.29	1.03	1.68
NGT_B-1000	98.45	0.68	0.87

Table S3. Comparison of ORR catalytic activity in 0.1 M KOH electrolyte with recently reported non-precious electrocatalysts in the literature.

Catalysts	Electrolyte	E_{onset}	$E_{1/2}$ (V)	Ref.
NGT_B-900	0.1 M KOH	1.06	0.89	This work
NCN-1000-5	0.1 M KOH	0.95	0.82	Energy Environ. Sci. 2019, 12, 322-333
NOGB-800	0.1 M KOH	0.92	0.84	Adv. Energy Mater. 2019, 1803867
NHC	0.1 M KOH	—	0.88	Nano Res. 2017, 10(4): 1163-1177
CF-K-A	0.1 M KOH	—	0.835	Small 2018, 14(21), 1800563
N-HPCNSs-800	0.1 M KOH	1.00	0.887	Nano Energy 49 (2018) 393-402
LHNHPC	0.1 M KOH	0.98	0.86	Appl. Catal. B-Environ., 210 (2017) 57-66
NPC-1000	0.1 M KOH	1.02	0.90	Adv. Funct. Mat., 27 (2017) 1606190
NDCF(Zn)-H2	0.1 M KOH	1.01	0.88	Small 2019, 15, 1805325
NDC-900	0.1 M KOH	0.86	0.76	J Mater Chem A. 2017;5(13):6025-6031.
1100-CNS	0.1 M KOH	0.94	0.85	Energy Environ. Sci. 2017;10(3):742-749
NPMC-1000	0.1 M KOH	0.94	0.85	Nat. Nanotech. 2015;10(5):444-452
NCF-900	0.1 M KOH	1.05	0.89	J. Mater. Chem. A, 2018, 6, 7762-7769
3D NCNT array	0.1 M KOH	0.93	0.81	Nano Energy 2017, 37, 98-107

Table S4. Comparison of the electrochemical performance of the NGT_B-900 electrode with performances of previously reported electrodes in 6 M KOH electrolyte.

Electrode materials	Surface area ($m^2\ g^{-1}$)	Specific capacitance ($F\ g^{-1}$)	Rate capability	Cycling	Ref.
N-OMCS	439	288 (1 A g^{-1})	66% at 50 A g^{-1}	100% (20000s)	Carbon, 2018, 127, 85-92
N-CNF	563	202 (1 A g^{-1})	82% at 30 A g^{-1}	97% (3000s)	ACS Nano 6 (2012) 7092-7102
graphene	2582	186 (1 A g^{-1})	58% at 10 A g^{-1}	93% (4000s)	Adv. Mater. 28 (2016) 5222-5228
N-MCS	2095	203 (1 A g^{-1})	95% at 20 A g^{-1}	100% (5000)	Nat. Commun. 6 (2015) 7221
N,S-OMC	1021	167 (1 A g^{-1})	60% at 50 A g^{-1}	97% (1000s)	J. Mater Chem. A 1 (2013) 7584-7591
OMC	781	157 (0.5 A g^{-1})	80% at 6 A g^{-1}	97% (20000s)	Nanoscale 6 (2014) 14657-14661
B-OMC	957	250 (1 A g^{-1})	60% at 5 A g^{-1}	92% (10000s)	Electrochim Acta 207 (2016)266-274
NPCs	806	323 (1 A g^{-1})	54% at 100 A g^{-1}	——	ACS Sustainable Chem. Eng., 2016, 4, 177-187
NPC□F	1375	364 (0.6 A g^{-1})	55% at 10 A g^{-1}	——	Adv. Mater., 2016, 28, 1981-1987
HNPCs	3700	289 (0.5 A g^{-1})	72% at 20 A g^{-1}	——	J. Mater. Chem. A, 2017, 5, 12958-12968
GF□NG	583	380 (0.6 A g^{-1})	63% at 80 A g^{-1}	——	Adv. Mater., 2017, 29, 1701677
NGT_B	1505	456 (1 A g^{-1})	76% at 50 A g^{-1}	94.5% (3000s)	This work

Table S5. Comparison of the performance of Zn-air batteries with various N-doped electrocatalysts.

Catalyst	Specific Capacity ($mAh\ g_{Zn}^{-1}$)	Energy Density ($Wh\ g_{Zn}^{-1}$)	Current density ($mA\ cm^{-2}$)	Ref.
SilkNC/KB	614.7	727.6	20	Chem. Mater., 2019, 31 1023-1029
BRCAC8502	732	----	10	ACS Sustain. Chem. Eng., 2019, 7, 17039-17046
NCN@CF2-950	720.5	900	10	ChemElectroChem, 2019, 6, 2924-2930
DCM-1000	815	915.46	50	Carbon, 2019, 145, 38-46
g-CN-CNF	363	388	10	Appl. Catal. B: Environ., 2018, 237, 140-148
NDGs-800	751	872.3	10	ACS Energy Lett., 2018, 3, 1183-1191
GSC-900	685	817	10	Energy, 2018, 143, 43-55
NPBC	760	850	5	Electrochim. Acta, 2017, 257, 250-258
DN-CP@G	591	---	20	Adv. Energy Mater., 2018, 8, 1703539
PAP-NCNCs	728	908	10	J. Mater. Chem. A, 2017, 5, 519-523
NDG	780	---	50	ACS Appl. Mater. Interfaces, 2017, 9, 7125-7130
BHPC-950	797	963	20	Adv. Funct. Mater., 2017, 27, 1701971
A-EPC-900	669	---	5	Chem. Commun, 2015, 51, 8841-88442

NCNF-1000	626	776	10	Adv Mater, 2016, 28, 3000-3006
N-CNF	615	760	10	Nano Energy, 2015, 11, 366-376
HPNSC	804	1007	10	J. Mater. Chem. A, 2019, 7, 9831-9836
NGT_B-900	813	1008	10	This work

References

(1) Shui, J. L.; Wang, M.; Du, F.; Dai, L. M., N-doped carbon nanomaterials are durable catalysts for oxygen reduction reaction in acidic fuel cells. *Sci. Adv.* **2015**, *1*, e1400129. DOI:10.1126/sciadv.1400129

(2) Ye, L.; Chai, G. L.; Wen, Z. H., Zn-MOF-74 Derived N-Doped Mesoporous Carbon as pH-Universal Electrocatalyst for Oxygen Reduction Reaction. *Adv. Funct. Mater.* **2017,** *27*, 1606190. DOI:10.1002/adfm.201606190

(3) Yazdi, A. Z.; Roberts, E. P. L.; Sundararaj, U., Nitrogen/sulfur co-doped helical graphene nanoribbons for efficient oxygen reduction in alkaline and acidic electrolytes. *Carbon* **2016,** *100*, 99-108. DOI:10.1016/j.carbon.2015.12.096

(4) Mamtani, K.; Jain, D.; Dogu, D.; Gustin, V.; Gunduz, S.; Co, A. C.; Ozkan, U. S., Insights into oxygen reduction reaction (ORR) and oxygen evolution reaction (OER) active sites for nitrogen-doped carbon nanostructures (CNx) in acidic media. *Appl. Catal. B-Environ.* **2018,** *220*, 88-97. DOI: 10.1016/j.apcatb.2017.07.086